

Numerical analyses of the nonequilibrium electron transport through the Kondo impurity beside the Toulouse point

Yoshihiro Nishiyama

*Department of Physics, Faculty of Science, Okayama University
Okayama 700-8530, Japan*

(Received)

E-mail: nisiyama@psun.phys.okayama-u.ac.jp

TEL: +81-86-251-7809

FAX: +81-86-251-7830

Abstract

Nonequilibrium electron transport through the Kondo impurity is investigated numerically for the system with twenty conduction-electron levels. The electron current under finite voltage drop is calculated in terms of the ‘conductance viewed as transmission’ picture proposed by Landauer. Here, we take into account the full transmission processes of both the many-body correlation and the hybridization amplitude up to infinite order. Our results demonstrate, for instance, how the exact solution of the differential conductance by Schiller and Hershfield obtained at the Toulouse point becomes deformed by more realistic interactions. The differential-conductance-peak height is suppressed below e^2/h with the width hardly changed through reducing the Kondo coupling from the Toulouse point, whereas it is kept unchanged by further increase of the coupling. We calculated the nonequilibrium local Green function as well. This clarifies the spectral property of the Kondo impurity driven far from equilibrium.

PACS codes/keywords: 72.15.Qm (Scattering mechanisms and Kondo effect), 82.20.Mj (Nonequilibrium kinetics), 75.40.Mg (Numerical simulation studies)

1 Introduction

Recently, in fine semiconductor devices, the Kondo effect has been observed at very low temperatures [1, 2, 3]. The indications of the Kondo effect are drawn mainly from the electron-transport measurements under various controlled system parameters such as the temperature, the gate voltage, the hybridization amplitude, the magnetic field and the bias voltage. In particular, the differential conductance $dI(V)/dV$ measured over a wide range of the bias voltage V shows a distinctive indication of the Kondo effect: The differential conductance shows a peak around the zero bias ($V = 0$) with the width comparable to the Kondo temperature. The peak height grows as the temperature is decreased. These features had been observed in various other experimental realizations such as tunnel metallic junctions and metallic point contacts [4, 5, 6, 7], although in these systems, the system parameters are not so freely tunable as in the semiconductor devices. Nevertheless, the series of experiments has been stimulating theoretical investigations so far [8, 9, 10, 11, 12, 13, 14, 15, 16, 17, 18, 19, 20, 21, 22, 23, 24, 25, 26, 27, 28]. The essence of the differential-conductance feature is attributed mainly to the shape of the local

density of states at the impurity. Note that the density of states contributes to the transmission probability in the intermediate stage of the transmission processes. It is well known that the density of states at the Kondo impurity is of a peak structure with the width comparable to the Kondo temperature. This picture yields comprehensive qualitative understanding of experimental observations.

Apart from the practical interest such as to explain the essential features of experimental observations, the subject may cast a rather fundamental problem where the many-body correlation and the nonequilibrium-driving force coexist, and are both important. Without the biquadratic correlation, we can calculate the nonequilibrium transport exactly [29] with the Keldysh approach [30]. On the other hand, the transport coefficient for correlated system is given by the Kubo formula, although the application is restricted in the vicinity of equilibrium. There have not yet been found any frameworks to command the nonequilibrium transport and the biquadratic correlation simultaneously. In fact, in the above mentioned theories, a number of perturbative approaches — either the voltage drop or the coupling to the leads are supposed to be infinitesimal — are employed. Recently, Schiller and Hershfield, however, succeeded in treating the situation rigorously [21, 23]. To the best of our knowledge, their solution is the first exact solution of a nonequilibrium correlated system. They found that the nonequilibrium Kondo model becomes integrable at the so-called Toulouse point [31], where the transverse and longitudinal Kondo couplings to both leads are tuned very carefully so as to satisfy the Emery-Kivelson condition [32]. Their result at zero temperature shows that the differential conductance is of a pure Lorentzian shape. This result might be rather disappointing, because the pure Lorentzian form had been known to be realized in simple quadratic system [29]. This rather uncharacteristic feature may be due to the fact that the system at the integrable point is nothing but quadratic. In fact, in a subsequent paper [22], they considered some perturbations to the Toulouse point, and tried to show how the integrable-point result is deformed by these perturbations.

Here, we formulate the nonequilibrium transport phenomenon with many-body correlation in a manner that is suitable for numerical simulation. Based on the formulation, we investigate the transport through the Kondo impurity. The transport coefficient is evaluated in terms of the ‘conductance viewed as the transmission’ picture proposed by Landauer [33, 34]. Here, we take into account the full transmission processes of both the many-body correlation and the hybridization amplitude up to infinite order. The rest of this paper is organized as follows. In the next section, we explain the model Hamiltonian, the so-called resonance level model, which is equivalent to the Kondo model [35, 36]. The equivalence is explained, and the advantages to investigate the former are explicated. In Section 3, the formulation of the nonequilibrium transport phenomenon, mentioned above briefly, is presented in detail. We also propose the algorithm to calculate the nonequilibrium Green function. In Section 4, we give the results of numerical simulation. In the last section, we give summary of this paper.

2 Resonance level model

In this section, we explain the so-called resonance level model. We simulated this model rather than the Kondo model. Although both models are equivalent [35, 36], it is much more advantageous to treat the former model rather than the latter. The Hamiltonian of the resonance level model is given by,

$$\mathcal{H} = \sum_k \left(v_F k + \frac{eV}{2} \right) L_k^\dagger L_k + \sum_k \left(v_F k - \frac{eV}{2} \right) R_k^\dagger R_k + V_h (S^+ c + S^- c^\dagger) + U S^z \frac{c^\dagger c - c c^\dagger}{2}. \quad (1)$$

The operator L_k^\dagger (R_k^\dagger) creates a conduction electron of wave number k in the left (right) lead. The wave number k is distributed uniformly over the range $k = -k_c \sim k_c$ ($k_c = \pi$); here, the wave number is indexed in such a way as $v_F k_i = 2i/(N-1) - 2/(N-1) - 1$ ($i = 1, 2, \dots, N$). That is, there are N conduction-electron levels in each lead. The parameter $v_F k_c (= \omega_c)$ is regarded as the unit of energy throughout this paper; namely, $v_F k_c = 1$. The operator c^\dagger

creates an electron at the impurity position; that is,

$$c^\dagger = \frac{1}{\sqrt{2N}} \sum_k (L_k^\dagger + R_k^\dagger). \quad (2)$$

The operators S^z and S^\pm are the conventional $S = 1/2$ spin operators. Hence, the parameters V_h and U denote the hybridization amplitude and the density-density correlation strength to the conduction-electron bands, respectively. Because we study the nonequilibrium situation where both leads are kept half-filled, the parameter eV give the chemical potential difference between two leads. The way how we realize such nonequilibrium situation in computer will be shown in the next section.

It is shown that the above model (1) is equivalent to the anisotropic Kondo Model by means of the bosonization technique [35, 36]. The anisotropic Kondo model is given by,

$$\begin{aligned} \mathcal{H}_K = & \sum_{k\sigma} \left(v_F k + \frac{eV}{2} \right) L_{k\sigma}^\dagger L_{k\sigma} + \sum_{k\sigma} \left(v_F k - \frac{eV}{2} \right) R_{k\sigma}^\dagger R_{k\sigma} \\ & + J_\parallel S^z \frac{c_\uparrow^\dagger c_\uparrow - c_\downarrow^\dagger c_\downarrow}{2} + J_\perp (S^+ c_\downarrow^\dagger c_\uparrow + S^- c_\uparrow^\dagger c_\downarrow), \end{aligned} \quad (3)$$

where the index σ denotes the spin index; $\sigma = \uparrow$ or \downarrow . According to the bosonization analysis, the following mapping relations should hold [36];

$$V = \frac{\rho_k J_\perp \omega_c}{2} (\rho_k \omega_c)^{-1/2}, \quad (4)$$

and,

$$U = (1 - \sqrt{2}|1 - \rho_k J_\parallel/2|)/2\rho_k, \quad (5)$$

with the density of states $\rho_k = (2\pi v_F)^{-1}$. The mapping relations tell the followings. First, at $J_\parallel = 2(1 - 1/\sqrt{2})/\rho_k$, there is a very special point at which the parameter U vanishes. (Note, however, that quantitative reliability of these mapping relations is *skeptical*. Precise connection between these models is somewhat lost in the bosonization procedure. Therefore, for instance, we cannot tell definitely at which point (V_h, U) the isotropic Kondo point is realized.) At this point, the resonance revel model (1) becomes quadratic, and this point, the so-called Toulouse point [31], corresponds to the strong-coupling fixed point of the Kondo model. Second, the reduction of the Kondo coupling from the Toulouse point corresponds to the attractive biquadratic correlation $U < 0$, whereas the furthermore increase of the Kondo coupling is viewed as the repulsive correlation $U > 0$. Roughly speaking, the previous rigorous analysis is concerned in the Toulouse point [21, 23]. In the analysis, however, the authors used the model with *two channel* density-density-correlation term, and arrived at the Toulouse point of the *two channel* Kondo model. Because our simulation is rather incapable of the two-channel Kondo physics, we have chosen the model with the conventional Kondo coupling. We investigate numerically the parameter region beside the Toulouse point $U = 0$ in Section 4.

We summarize below the advantages to treat the resonance level model rather than the Kondo model: First, in the former model, the spin index is dropped so that we can diagonalize the system size twice as large as that of the Kondo model. The physical reason of this dropping is originated in the followings. Because the Kondo problem is essentially of a one-dimensional problem, The charge and spin degrees of freedom are separated completely. Therefore, only the spin degrees of freedom are subjected to the impurity-spin scattering. That is, the spin degrees of freedom transmit through the impurity through the assistance of the scattering, whereas the charge degrees of freedom do not transmit at all. That is why we can ignore the charge sector. (Therefore, the perfect-transmission conductance is *not* $2e^2/h$, which arises in conventional models, but e^2/h , because the charge-sector transmission is ignored completely here.) Secondly, as is discussed in the previous paragraph, it is very advantageous that we can start from the Kondo fixed point, namely, the Toulouse point, which readily contains the very essence of the Kondo physics. Hence, we can study the effect of the biquadratic term in a systematic manner as the gradual deviation from the fixed point.

3 Formulation of the nonequilibrium electron transport

In this section, we discuss how we set up the formalism to simulate the nonequilibrium electron-transport phenomenon. The formalism is prepared in such a way that it is readily implemented in a computer-simulation algorithm. First, we give a conductance formula based on the ‘conductance viewed as transmission’ picture proposed by Landauer [33, 34]. Extensive use of numerical technique enables the evaluation of the transition-matrix elements containing higher order contributions of both the hybridization amplitude and the density-density correlation. Then, we give the algorithm to calculate the nonequilibrium Green function, which is useful in order to investigate the spectral property under nonequilibrium current flow.

According to the Landauer picture, the electron current is given by the transmission probability between two leads;

$$\begin{aligned}
I &= e \sum_{kk'} \left\{ f(v_F k) \frac{2\pi}{\hbar} |T_{kk'}|^2 (1 - f(v_F k')) \delta(v_F k - v_F k' + eV) \right. \\
&\quad \left. - (1 - f(v_F k)) \frac{2\pi}{\hbar} |T_{kk'}|^2 f(v_F k') \delta(v_F k - v_F k' + eV) \right\} \\
&= eN^2 \rho_\varepsilon^2 \int d\varepsilon \left\{ f(\varepsilon - eV) \frac{2\pi}{\hbar} |T_{\varepsilon - eV, \varepsilon}|^2 (1 - f(\varepsilon)) - (1 - f(\varepsilon - eV)) \frac{2\pi}{\hbar} |T_{\varepsilon - eV, \varepsilon}|^2 f(\varepsilon) \right\} \\
&= eN^2 \rho_\varepsilon^2 \int_{-eV/2}^{eV/2} d\varepsilon \frac{2\pi}{\hbar} |T_{\varepsilon - eV/2, \varepsilon + eV/2}|^2. \tag{6}
\end{aligned}$$

We have used the Fermi-distribution function $f(\varepsilon)$ and the density of states $\rho_\varepsilon = 1/2$, and supposed that the system is at zero temperature. $T_{kk'}$ denotes the transition-matrix element from the wave number k of the left lead to k' of the right lead. The explicit expression of $T_{kk'}$ is considered afterwards. Thereby, we obtain the differential conductance,

$$\begin{aligned}
G(eV) &= \frac{d}{dV} I \\
&= \frac{d}{dV} eN^2 \rho_\varepsilon^2 \int_{-eV/2}^{eV/2} d\varepsilon \frac{2\pi}{\hbar} |T_{\varepsilon - eV/2, \varepsilon + eV/2}|^2. \tag{7}
\end{aligned}$$

Therefore, the conductance $G(eV)$ is given by the derivative of the integral of the following integrand,

$$g(\varepsilon) = eN^2 \rho_\varepsilon^2 \frac{2\pi}{\hbar} |T_{\varepsilon - eV/2, \varepsilon + eV/2}|^2. \tag{8}$$

(Note that the function $g(\varepsilon)$ is an even function because of the particle-hole symmetry.) Hence, it is expected that the integrand $g(\varepsilon)$ yields the conductance,

$$G(eV) \simeq e g(eV/2), \tag{9}$$

unless the integrand depends on eV very much. Fortunately, it is known that in the noninteracting case $U = 0$, the current is expressed in terms of the following rigorous form [29],

$$I = \frac{2\pi e (V_h/\sqrt{2})^4}{\hbar} \int_{-eV/2}^{eV/2} d\omega |\mathcal{G}(\omega)|^2 \rho_\varepsilon^2. \tag{10}$$

(That is, at $U = 0$, the transition matrix $T_{\varepsilon - eV/2, \varepsilon + eV/2}$ is related to the local Green function at the impurity site ($\propto \mathcal{G}(\omega = \varepsilon)$.) Because the integrand is *completely* independent on eV , the relation (9) holds exactly. We expect that beside $U = 0$, the relation continues to hold well. In fact, as is presented afterwards in Section 4.3, $\omega (= \varepsilon)$ -dependence is dominated and determines the essential feature (peak structure) of the integrand, whereas eV just causes sub-dominant detailed contributions. As is shown below, a handy formula (26) for conductance estimate exists and is expressed in the similar form as ours (6). In the presence of U , the integrand behaviors

of ours (6) and the formula (6) become *qualitatively* different. Therefore, at the present stage, it would be well worth considering the conductance in the approximation level of (9).

Next, we calculate the transition-matrix element. In order to do that, we must prepare the initial and final states,

$$|i\rangle = L_{k_{N/2+1}}^\dagger |g_0\rangle, \quad (11)$$

and

$$|f\rangle = R_{k_j}^\dagger |g_0\rangle \quad (j = N/2 + 1, N/2 + 2, \dots, N), \quad (12)$$

respectively. We have supposed that N is an even integer. The state $|g_0\rangle$ represent the situation where both leads are half-filled;

$$|g_0\rangle = L_{k_1}^\dagger L_{k_2}^\dagger \cdots L_{k_{N/2}}^\dagger R_{k_1}^\dagger R_{k_2}^\dagger \cdots R_{k_{N/2}}^\dagger |0\rangle. \quad (13)$$

In the single-particle transmission process, the energy should be conserved. This conservation condition restricts the available values of the voltage drop within the series $eV = 2(j - N/2 - 1)/(N - 1)$ ($j = N/2 + 1, N/2 + 2, \dots, N$); note that our conduction-electron band is discrete. With use of these initial and final states, we obtain the transition probability,

$$w_{i \rightarrow f} = \frac{d}{dt} |c_f(t)|^2 \Big|_{t=0}, \quad (14)$$

with,

$$c_f(t) = \langle f | \frac{U_{I\eta}(t, -\infty) |i\rangle}{|U_{I\eta}(t, -\infty) |i\rangle}. \quad (15)$$

In the above, $U_{I\eta}$ is the time-evolution operator of the interaction representation;

$$U_{I\eta}(t_2, t_1) = \text{Te}^{-i \int_{t_1}^{t_2} dt \mathcal{H}_1(t)/\hbar}, \quad (16)$$

with,

$$\mathcal{H}_1(t) = e^{i\mathcal{H}_0 t/\hbar} \left(V_h (S^+ c + S^- c^\dagger) + U S^z \frac{c^\dagger c - c^\dagger c}{2} \right) e^{-i(\mathcal{H}_0 + i\eta)t/\hbar}, \quad (17)$$

and,

$$\mathcal{H}_0 = \sum_k \left(v_F k + \frac{eV}{2} \right) L_k^\dagger L_k + \sum_k \left(v_F k - \frac{eV}{2} \right) R_k^\dagger R_k. \quad (18)$$

($\mathcal{H} = \mathcal{H}_0 + \mathcal{H}_1$.) The normalization factor in eq. (15) is vital, because the infinitesimal damping parameter η violates the unitarity of $U_{I\eta}$. This fact is known as the Gell-Mann-Low theorem [37]. Moreover, it is notable that η plays a significant role to realize ‘nonequilibrium dissipative state’ breaking the time-reversal symmetry [38]. Using the property of the time-evolution operator $U_{I\eta}$, we obtain the following expression,

$$\begin{aligned} w_{i \rightarrow f} &= \frac{d}{dt} \frac{|\langle f | U_{I\eta}(t, -\infty) |i\rangle|^2}{\langle i | U_{I\eta}(\infty, t) U_{I\eta}(t, -\infty) |i\rangle} \Big|_{t=0} \\ &= \frac{d}{dt} \frac{|\langle f | U_{I\eta}(t, -\infty) |i\rangle|^2}{\langle i | U_{I\eta}(\infty, -\infty) |i\rangle} \Big|_{t=0} \\ &= \frac{1}{|U_{I\eta}(0, -\infty) |i\rangle^2} \frac{d}{dt} |\langle f | U_{I\eta}(t, -\infty) |i\rangle|^2 \Big|_{t=0}. \end{aligned} \quad (19)$$

Through expanding the operator $U_{I\eta}$ into the Dyson series, one arrives at the following formula,

$$w_{i \rightarrow f} = \frac{2\pi}{\hbar} |\langle f | T | i \rangle|^2 \delta(E_f - E_i), \quad (20)$$

where the transition matrix T is,

$$T = \frac{1}{|U_{I\eta}(0, -\infty) |i\rangle} \mathcal{H}_1 \left(1 - \frac{1}{\mathcal{H}_0 + \mathcal{H}_1 - E_i - i\eta} \mathcal{H}_1 \right), \quad (21)$$

with $\mathcal{H}_0|\text{i}\rangle = E_{\text{i}}|\text{i}\rangle$ and,

$$U_{\text{I}\eta}(0, -\infty)|\text{i}\rangle = \left(1 - \frac{1}{\mathcal{H}_0 + \mathcal{H}_1 - E_i - i\eta}\mathcal{H}_1\right)|\text{i}\rangle. \quad (22)$$

The above formulae complete our technique to compute the electron conductance; note the relation $T_{0,eV} = \langle \text{f}|T|\text{i}\rangle$. Readers may have noticed that we are subjected to the Lippmann-Schwinger formulation essentially [38]. It is notable that the formula for the transition matrix (21) contains *infinite-order contributions* with respect to \mathcal{H}_1 , and thus our simulation does *not* resort to any perturbative treatments.

Lastly, we show the way to calculate the non-equilibrium Green function,

$$\begin{aligned} \mathcal{G}(eV, \omega) &= \int dt e^{i\omega t} \mathcal{G}(eV, t) \\ \mathcal{G}(eV, t) &= -i\Theta(t)\langle g_{eV}|4\{S^-(t), S^+\}|g_{eV}\rangle, \end{aligned} \quad (23)$$

where the nonequilibrium steady state is given by,

$$|g_{eV}\rangle = \frac{U_{\text{I}\eta}(0, -\infty)|g_0\rangle}{|U_{\text{I}\eta}(0, -\infty)|g_0\rangle}. \quad (24)$$

Because of the same reasoning as the above, we need a normalization factor. The time-evolved state is calculated similarly,

$$U_{\text{I}\eta}(0, -\infty)|g_0\rangle = \left(1 - \frac{1}{\mathcal{H}_0 + \mathcal{H}_1 - E_{g0} - i\eta}\mathcal{H}_1\right)|g_0\rangle. \quad (25)$$

This gives an explicit expression for the state $|g_{eV}\rangle$. What is still left is to calculate the Fourier transform of the time correlation function of eq. (23). At first glance, one might think that it is impossible, because all the eigenstates are needed to evolve the time correlation. Gagliano and Balseiro, however, invented a way to express the Green function (23) in a compact continued-fraction form with the Lanczos tri-diagonal elements [39]. Through utilizing their technique, the scheme to calculate nonequilibrium Green function is completed. We emphasize that in our scheme, we do not resort to any perturbative treatments.

The Green function is useful to estimate approximate value of electron current. So far, the following formula has been used to obtain the nonequilibrium current;

$$I = \frac{e}{\hbar} \int_{-eV/2}^{eV/2} d\omega \frac{\Gamma^L \Gamma^R}{\Gamma^L + \Gamma^R} \cdot \frac{-1}{\pi} \text{Im}\mathcal{G}(eV, \omega), \quad (26)$$

with the Abrikosov-Suhl resonance frequency for each lead [15, 16], namely,

$$\Gamma^{\text{L,R}} = 2\pi\rho_{\varepsilon}(V_{\text{h}}/\sqrt{2})^2. \quad (27)$$

As is mentioned in Introduction, this formula (26) insists that the spectral density at the impurity site ($\propto \text{Im}\mathcal{G}$) contributes to the current flow. Note that as in our above-mentioned formula (6), the current is expressed in terms of an integral form. An so, because of the same reasoning mentioned before, the integrand of (26) does hardly depend on eV for $U \approx 0$, yielding a compact expression for the differential conductance;

$$G(eV) \simeq \frac{e^2}{\hbar} \cdot \frac{\Gamma^L \Gamma^R}{\Gamma^L + \Gamma^R} \cdot \frac{-1}{\pi} \text{Im}\mathcal{G}(eV, \omega = eV/2), \quad (28)$$

In the next section, we report that the conductance estimate with our formula (9) differs qualitatively from that of the above handy relation.

4 Numerical results and discussions

So far, we have prepared prescriptions for simulating the nonequilibrium electron transport numerically. In this section, we carry out numerical simulations based on the prescriptions.

4.1 Preliminaries of our numerical simulation

Here, we summarize details of our numerical computation. We simulated the system consisting of twenty conduction-electron levels. (The form of the Hamiltonian is explained in Section 2; see eq. (1).) That is, there are ten levels for each lead; $N = 10$. (Owing to the presence of the density-density-correlation term in the Hamiltonian (1), the Hamiltonian-matrix elements are not so sparse as in conventional diagonalization simulations. That costs considerable computation time, even though the dimensionality of the Hilbert space ($\sim 2^{21}$) is not so particularly overwhelming.)

The most important computation stage is that to evaluate the resolvent which is appearing in eqs. (21) and (22). The resolvent is computed with the conjugate-gradient algorithm. The convergence of the conjugate-gradient iteration is not very stable. This instability becomes more serious as the coupling to the leads is strengthened. This instability has been encountered so far in general in calculating resolvent of many-body problem numerically. Here, we have used the following new trick to overcome this difficulty. We substituted the parameter η in eqs. (21) and (22) with,

$$\eta = \eta^{(0)} + \eta^{(2)} \sum_k ((v_F k)^2 L_k^\dagger L_k + (v_F k)^2 R_k^\dagger R_k). \quad (29)$$

Now, η is not a c-number constant, but is an operator. Because the parameter determines the energy resolution, it should be of the order of the conduction-band discrete spacing. Hence, we set $\eta^{(0)} = 0.1$. The first term alone results in a desperate instability of numerical procedure. Hence, we have added the second new term. The meaning of this term may be transparent: The term enforces the life time of each conduction-band level to vary as the square of the excitation energy measured from the Fermi level. Such dependence might be reasonable, because the Landau theory for the interacting electron gas concludes the same dependence of the life time. Here, we set $\eta^{(2)} = 0.06$ for $V_h = 0.3$.

We found that this choice of parameters is the best one: Reader may feel that our $N = 10$ -level approximation of the conduction band might be serious, because the Fermi-surface singularity is important to realize the Kondo effect. Yet, owing to the resonance-level-model mapping, we are actually in the *strong*-Kondo-coupling regime (Toulouse point), where the Kondo temperature is given by $\sim \Gamma^L + \Gamma^R = 2\pi\rho_\varepsilon V_h^2$; see eq. (27). As a matter of fact, our choice of $V_h = 0.3$ gives the Kondo temperature ~ 0.28 which is larger than the conduction-band level spacing $2/N = 0.2$. On the contrary, the energy-resolution broadening term η is not negligible compared with the Kondo temperature so that we are suffered from a broadening of the zero-bias-anomaly peak. We found that for $V_h > 0.3$, the numerical instability becomes desperately serious, and exceedingly large smearing factor η is needed. Hence, we concentrated ourselves on the above-mentioned parameter point with $V_h = 0.3$, $\eta^{(0)} = 0.1$ and $\eta^{(2)} = 0.06$, where we can achieve the Kondo effect and barely manage the numerical instability with a modest energy-resolution broadening.

4.2 Differential conductance

In this subsection, we present our numerical result of the differential conductance. The calculation is based on the formula (9). We discuss the result with an emphasis on the effect of U , namely, the deviation from the Toulouse point.

In Fig. 1, we plotted the differential conductance against the voltage drop eV for $V_h = 0.3$ and various U . We see that the differential conductance is maximal at the zero bias $eV = 0$ irrespective of U . This peak structure is known as the ‘zero-bias anomaly.’ The anomaly has been observed experimentally, and is very significant to confirm that the electron actually tunnels between two leads with a certain quantum-mechanical tunneling amplitude.

First, we discuss the data for $U = 0$ (the Toulouse point). At this quadratic case $U = 0$, an analytical prediction for the differential conductance is available; see Section 3. According to

that, the differential conductance is given by the formula (28) with the Green function,

$$\mathcal{G}(\omega) = \frac{1}{\omega + \delta - \sum_k \frac{(V_h/\sqrt{2N})^2}{\omega + \delta - v_F k - eV/2} - \sum_k \frac{(V_h/\sqrt{2N})^2}{\omega + \delta - v_F k + eV/2}}. \quad (30)$$

The result of this formula with $\delta = 0.05$ is also plotted as a dashed line in Fig. 1. We see that our numerical result succeeds in reproducing the zero-bias conductance $\sim e^2/h$, which is accordant with the Landauer theory, and the zero-bias peak as well. On the contrary, our zero-bias-peak width is broadened substantially compared with the analytical prediction curve. That is due to the energy-resolution-smearing factor η (29), which cannot be omitted in order to stabilize the conjugate-gradient procedure. (This factor η broadens the energy resolution, and loosens the energy-conservation constraint. Thereby, this parameter enhances the transmission probability, resulting in an enhanced estimate of conductance.) As is explicated in Section 4.1, we had implemented a new trick that the factor η (life time) is not a constant, but is gained near the band edges. Therefore, owing to η , our conductance data suffer a correction and are enhanced especially for large potential drop $eV \sim 1$. Hence, we rather focus our attention on the qualitative variation of the conductance curve $G(eV)$ due to the introduction of the many-body correlation U . It should be stressed that, as is explained in Section 3, besides this broadening, our simulation is free from any approximations, and actually, takes into account full many-body correlation processes.

Second, keeping that in mind, let us turn to the case of $U < 0$. Note that the case $U < 0$ corresponds to the situation where the Kondo coupling is reduced from the value of the Toulouse point; refer to the mapping relations (4). In Fig. 1, we see that the zero-bias conductance is suppressed significantly by the reduction of the Kondo coupling. It is very surprising, because conventional picture based on the one-particle description, namely, eqs. (28) and (27), gives the conductance e^2/h irrespective of the hybridization amplitude as far as the left-right hybridization couplings are symmetric. Therefore, we notice that such reduction is of a nontrivial many-body effect, and in principle, that should be managed by *ab initio* treatments such as ours. As a matter of fact, a conductance estimate based on the convenient formula (28) gives qualitatively opposite behavior that the conductance is *enhanced* with $U < 0$; this discrepancy is reported in the next subsection.

Furthermore, it seems that the width of the zero-bias-anomaly peak is not changed very much by $U < 0$. It may be interesting to compare our findings with those of the lowest-order-perturbation theory with respect to the Toulouse point by Majumdar, Schiller and Hershfield [22]. They studied the effect of certain three types of perturbations to the differential conductance. These perturbations are thought to drive the integrable Toulouse Hamiltonian in the direction of the weak Kondo coupling; namely, more realistic coupling. (Because they are employing a field-theoretical description together with a very sophisticated canonical transformation, the origin of these perturbations in the language of the original Kondo Hamiltonian is rather unclear, and is to be clarified.) They found that some two perturbations keep the height fixed, but sharpen the width, whereas the other perturbation suppresses the height with the width unchanged. The true effect is speculated to be a certain mixture of those effects. Our results suggest that the reduction of the Kondo coupling reduces the height, but does not change the width very much; that is, in the field-theoretical language [22], the latter type of perturbation might be realized actually in the physics of $U < 0$.

Next, we discuss the case $U > 0$. This repulsive density-density correlation is interpreted as the *very* strong Kondo coupling, which is even exceeding the Toulouse-coupling strength. Hence, this case might not be so relevant in the language of the Kondo physics, and has not yet been studied very well [40]. Nevertheless, apart from the context of the Kondo problem, this situation is interesting by its own right. In Fig. 1, We observe that as the repulsive correlation is increased, no particular change is observed for the differential conductance especially for $eV \sim 0$. That is, despite of the repulsion, inherent quantum-mechanical resonance restores the hybridization between the impurity and the conduction electron. This situation will be more clarified in the next subsection through referring to the spectral-function data.

4.3 Nonequilibrium Green function

In this subsection, we present the numerical result of the nonequilibrium Green function. The calculation is based on the formula (23). We concentrate on the imaginary part of the Green function, which yields the local density of states at the impurity site;

$$\rho(\omega) = -\frac{1}{\pi} \text{Im} \mathcal{G}(eV, \omega + i\delta), \quad (31)$$

with $\delta = 0.1$. Once the spectral function is obtained, one can adopt the handy formula (28) to estimate the conductance. We show that the estimates (behaviors) differ qualitatively from our first-principle results shown in Section 4.2.

In Figs. 2-4, we plotted the density of states for $V_h = 0.3$, and $U = 0, 0.2$ and -0.2 , respectively. The local density of states shows a peak structure. That is, the impurity level is smeared out by the mixing (resonance) to the conduction-electron band. The peak width corresponds to the inverse of the life time of the impurity state.

First, we discuss the case of $U = 0$ (Fig. 2). We see that the local density of states, namely, the resonance peak, is suppressed gradually as the bias voltage eV is increased. That is understood as follows: For $eV \sim \omega_c (= 1)$, the Fermi-energy position approaches the band edge. In that case, the resonance is not fully formed because of the disturbance of the band edge. That causes the reduction of the resonance peak for $eV \sim 1$.

Second, let us turn to the cases with the many-body correlation $U \neq 0$. In those cases, the Green function becomes far more nontrivial, and contains significant informations. For $U = 0.2$ (Fig. 3), the density of states forms broader resonance than that of $U = 0$. In particular, the sub-peaks at $\omega = \pm eV/2$ are prominent; note that the frequencies $\omega = \pm eV/2$ are the Fermi levels of the leads. The sub-peak height stays aloft even for $eV > 0$. Thereby, the sub-peaks constitute shoulders of the main peak, resulting in considerable broadening of the main peak. This feature has been captured by previous studies [16, 17, 28], and is speculated to be the very essence of the nonequilibrium Kondo physics. We emphasize that the present simulation does actually capture this characteristic without resorting to any approximations. This prominent resonance may be the precursor of the unexpected large conductance, which we reported in the previous subsection. On the other hand, for $U = -0.2$ (Fig. 4), the density of states forms a very narrow peak, and the shoulders at $\omega = \pm eV/2$ are not grown very much. That is, in this weak Kondo coupling case, the Kondo resonance is suppressed to a considerable extent. This is consistent with the observation of the previous subsection that the (zero-bias) conductance is suppressed significantly by $U < 0$.

Finally, we show the result of the differential conductance based on the approximative formula (28). The application of the formula is now possible, because we have nonequilibrium-Green-function data. The result is plotted in Fig. 5, Although this approximative formula reproduces the zero-bias anomaly, the dependence on U differs significantly from that of our first-principle result. For instance, in Fig. 5, the conductance is *increased* by $U < 0$, whereas it should be suppressed according to our simulation. (Our conclusion may also be supported by a recent report, where, however, the authors studied the tunneling amplitude from one edge to the bulk of the Hubbard chain [40].) It is suspected that the approximate formula does not fully include the many-body correlation effect. One cannot expect, as a matter of fact, that the nonequilibrium transport coefficient is given by one-particle Green function alone, because the Kubo theory tells that the *non*-linear-response function should be expressed in terms of *many*-point Green functions.

5 Summary

We have investigated numerically the nonequilibrium electron transport through the Kondo impurity. In this problem, nonequilibrium-driving force and biquadratic correlation coexist, and both are playing a crucial role. For the first time, we succeeded in simulating the situation without resorting to any perturbative treatments. Moreover, because we utilized the mapping to

the resonance level model, we could clarify the effect of the biquadratic correlation as a gradual deviation from the Toulouse point. We calculated the differential conductance with the formula (9) and the nonequilibrium Green function with eq. (23). Our results tell that the effect of the biquadratic interaction lies out of the scope of the one-particle description: The attractive density-density coupling, which corresponds to a reduced Kondo coupling from the Toulouse point, suppresses the zero-bias conductance below the Landauer value. The width of the zero-bias anomaly, on the other hand, is not changed very much. The above is to be contrasted with the field-theoretical lowest-order-perturbation theory with respect to the Toulouse point [22]. The repulsive coupling, on the contrary, does not influence the conductance. The above features are supported by our spectral function data based on eq. (31).

We stress that as we have demonstrated, the ‘steady nonequilibrium’ transport can be simulated without carrying out any time-evolution simulations. The formalism and the implementation to the computer algorithm, which are demonstrated here, are readily applicable to other wide class of steady nonequilibrium transport with many-body interaction. As is clarified here, in such situation as well, the many-body correlation would cause new unexpected behavior. This would be remained in future.

Acknowledgments

The author is grateful to Prof. W. Apel and Prof. H.-U. Everts for helpful discussions. Hospitality at Institut für Theoretische Physik, Universität Hannover, is gratefully acknowledged.

References

- [1] D. Goldhaber-Gordon, H. Shtrikman, D. Mahalu, D. Abusch-Magder, U. Meirav and M. A. Kastner: *Nature* **391** (1998) 156.
- [2] S. M. Cronenwett, T. H. Oosterkamp and L. P. Kouwenhoven: *Science* **281** (1998) 540.
- [3] J. Schmid, J. Weis, K. Eberl and K. v. Klitzing: *Physica B* **256-258** (1998) 182.
- [4] A. F. G. Wyatt: *Phys. Rev. Lett.* **13** (1964) 401.
- [5] R. A. Logan and J. M. Rowell: *Phys. Rev. Lett.* **13** (1964) 404.
- [6] S. Gregory: *Phys. Rev. Lett.* **68** (1992) 2070.
- [7] D. C. Ralph and R. A. Buhrman: *Phys. Rev. Lett.* **72** (1994) 3401.
- [8] J. Appelbaum: *Phys. Rev. Lett.* **17** (1966) 91.
- [9] P. W. Anderson: *Phys. Rev. Lett.* **17** (1966) 95.
- [10] L. I. Glazman and M. É. Raikh: *JETP Lett.* **47** (1988) 452.
- [11] T. K. Ng and P. A. Lee: *Phys. Rev. Lett.* **61** (1988) 1768.
- [12] A. Kawabata: *J. Phys. Soc. Japan* **60** (1991) 3222.
- [13] A. Kawabata: *J. Phys. Soc. Japan* **67** (1998) 2430
- [14] Y. Meir, N. S. Wingreen and P. A. Lee: *Phys. Rev. Lett.* **66** (1991) 3048.
- [15] Y. Meir and N. S. Wingreen: *Phys. Rev. Lett.* **68** (1992) 2512.
- [16] Y. Meir, and N. S. Wingreen and P. A. Lee: *Phys. Rev. Lett.* **70** (1993) 2601.
- [17] T. K. Ng: *Phys. Rev. Lett.* **70** (1993) 3635.

- [18] N. S. Wingreen and Y. Meir: Phys. Rev. B **49** (1994) 11040.
- [19] S. Hershfield, J. H. Davies and J. W. Wilkins: Phys. Rev. Lett. **67** (1991) 3720.
- [20] S. Hershfield, J. H. Davies and J. W. Wilkins: Phys. Rev. B **46** (1992) 7046.
- [21] A. Schiller and S. Hershfield: Phys. Rev. B **51** (1995) 12896.
- [22] K. Majumdar, A. Schiller and S. Hershfield. Phys. Rev. B **57** (1998) 2991.
- [23] A. Schiller and S. Hershfield: Phys. Rev. B **58** (1998) 14978.
- [24] T. Inoshita, A. Shimizu, Y. Kuramoto and H. Sakaki: Phys. Rev. B **48** (1993) 14725.
- [25] W. Izumida, O. Sakai and Y. Shimizu: J. Phys. Soc. Japan **67** (1998) 2444.
- [26] A. Oguri, H. Ishii and T. Saso: Phys. Rev. B **51** (1995) 4715.
- [27] A. Oguri: Phys. Rev. B **56** (1997) 13422; (E) **58** (1998) 1690.
- [28] J. König, H. Schoeller and G. Schön: Phys. Rev. Lett. **76** (1996) 1715.
- [29] C. Caroli, R. Combescot, P. Nozieres and D. Saint-James: J. Phys. C: Solid St. Phys. **4** (1971) 916.
- [30] L. V. Keldysh: Sov. Phys.-JETP **20** (1965) 1018.
- [31] G. Toulouse: Phys. Rev. B **2** (1970) 270.
- [32] V. J. Emery and S. A. Kivelson: Phys. Rev. B **46** (1992) 10812.
- [33] R. Landauer: IBM J. Res. Dev. **1** (1957) 223.
- [34] Y. Imry and R. Landauer: Rev. Mod. Phys. **71** (1999) S306.
- [35] P. Schlottmann: Phys. Rev. B **25** (1982) 4815.
- [36] F. Guinea, V. Hakim and A. Muramatsu: Phys. Rev. B **32** (1985) 4410.
- [37] M. Gell-Mann and F. Low: Phys. Rev. **84** (1951) 350.
- [38] S. Hershfield: Phys. Rev. Lett. **70** (1993) 2134.
- [39] E. R. Gagliano, C. A. Balseiro: Phys. Rev. Lett. **59** (1987) 2999.
- [40] G. Bedürftig and H. Frahm: preprint.

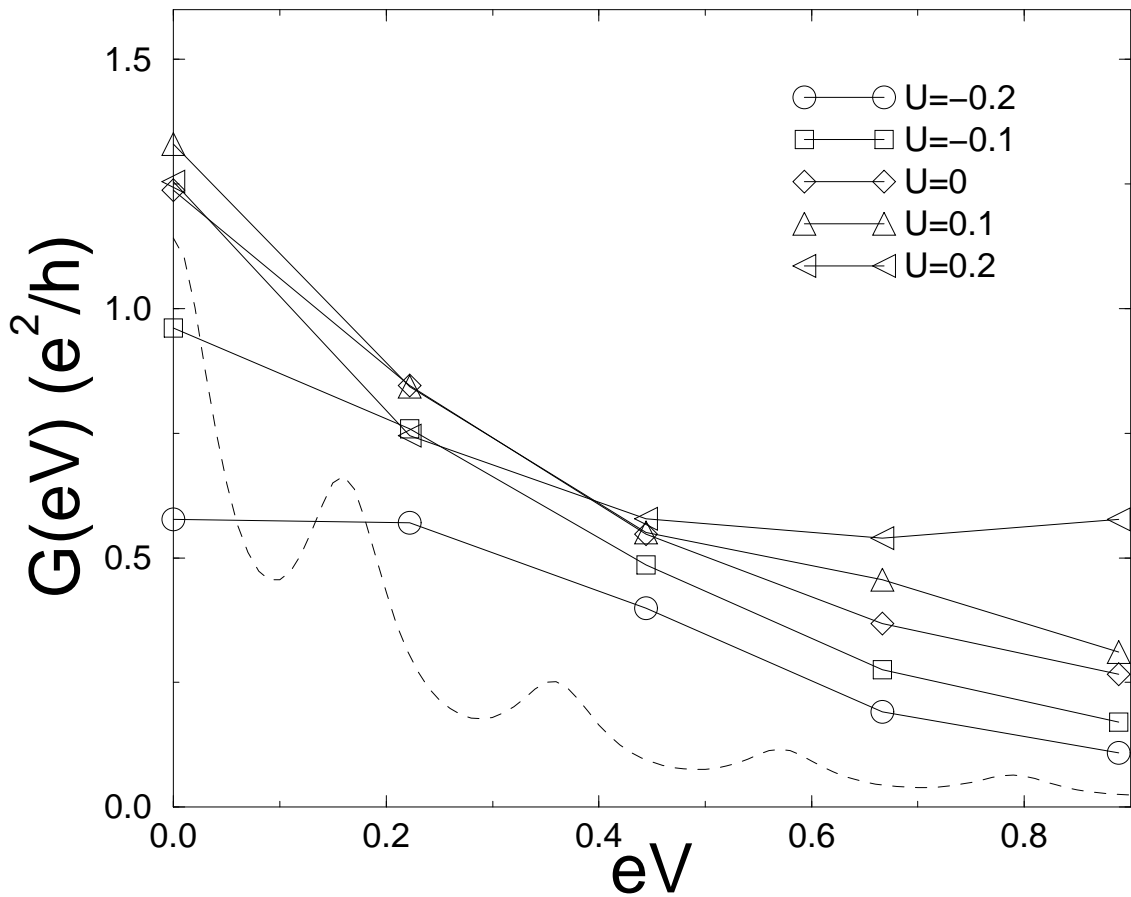


Figure 1: Differential conductance (9) is plotted for $V_h = 0.3$ and various U . The dashed curve shows the result with the analytic formula (28) that is valid at $U = 0$.

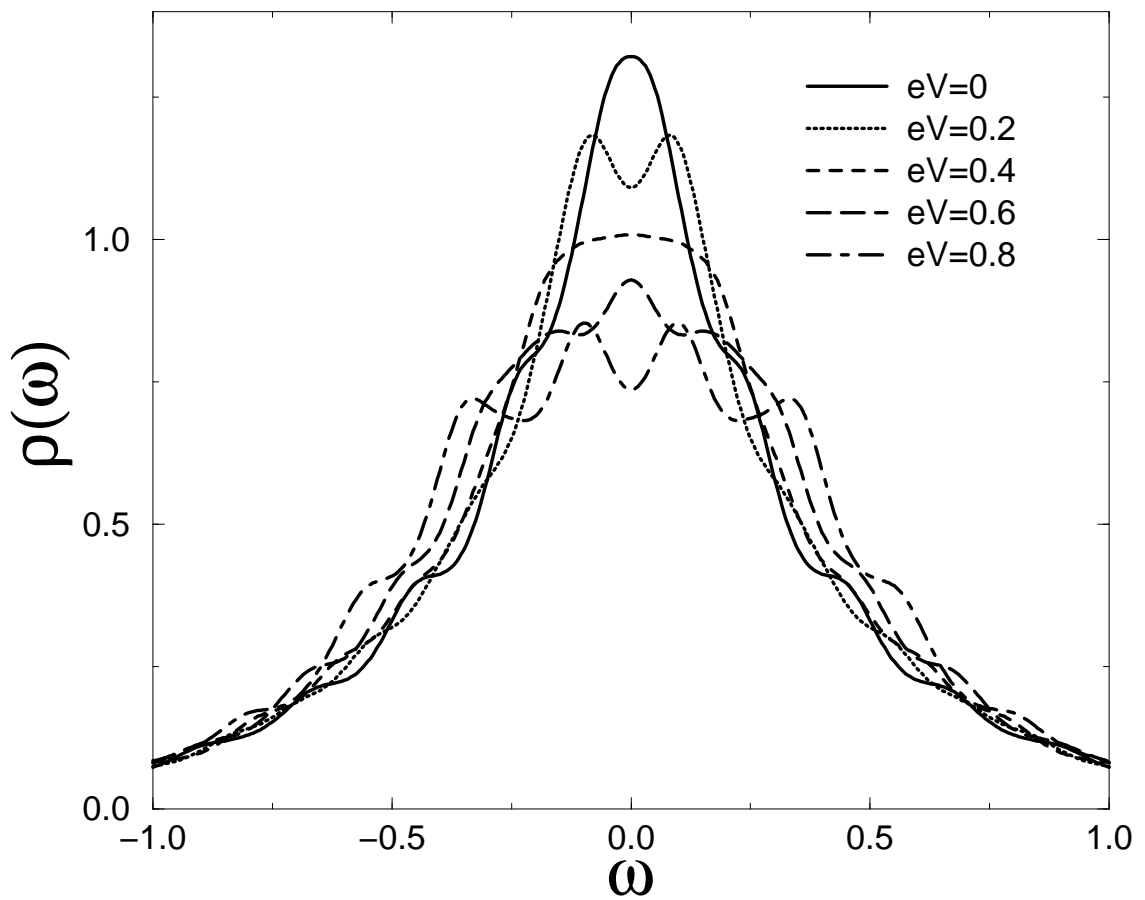


Figure 2: Local density of states at the impurity site (31) for $V_h = 0.3$ and $U = 0$.

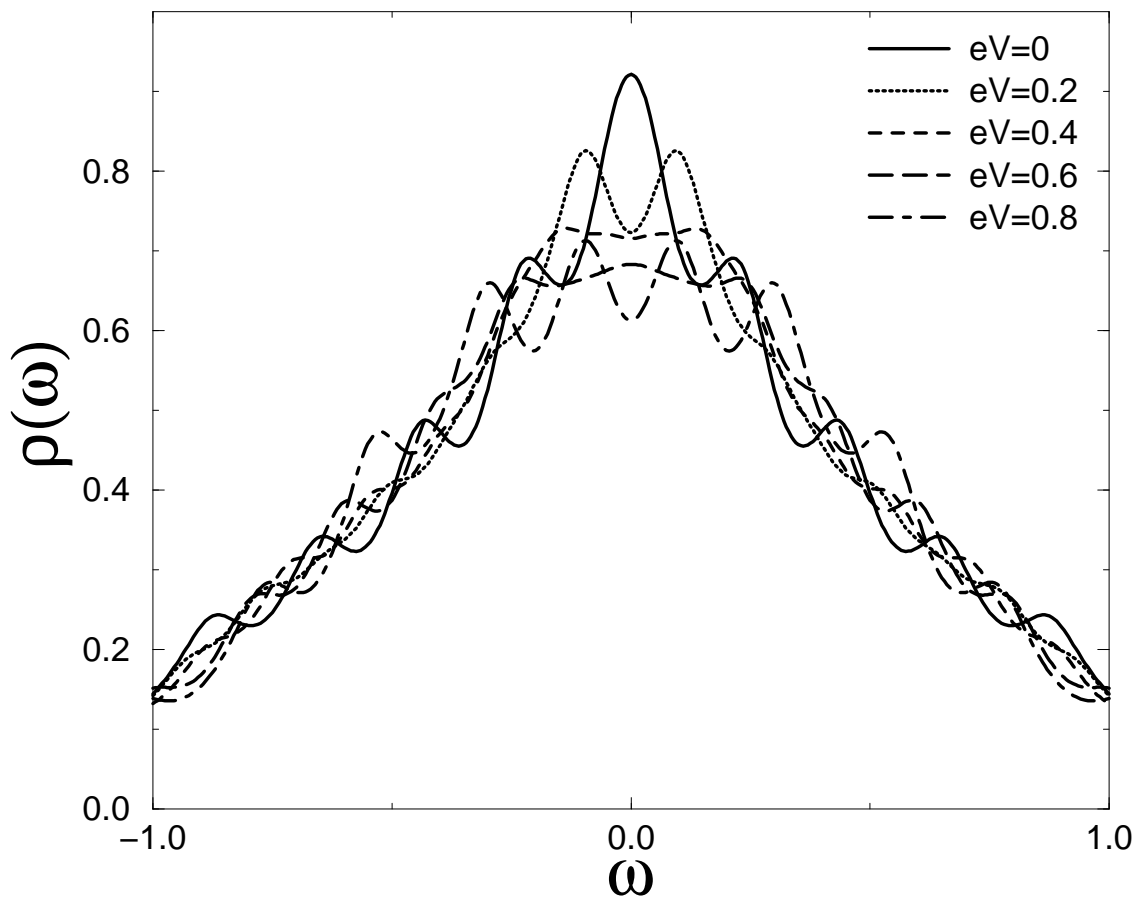


Figure 3: Local density of states at the impurity site (31) for $V_h = 0.3$ and $U = 0.2$.

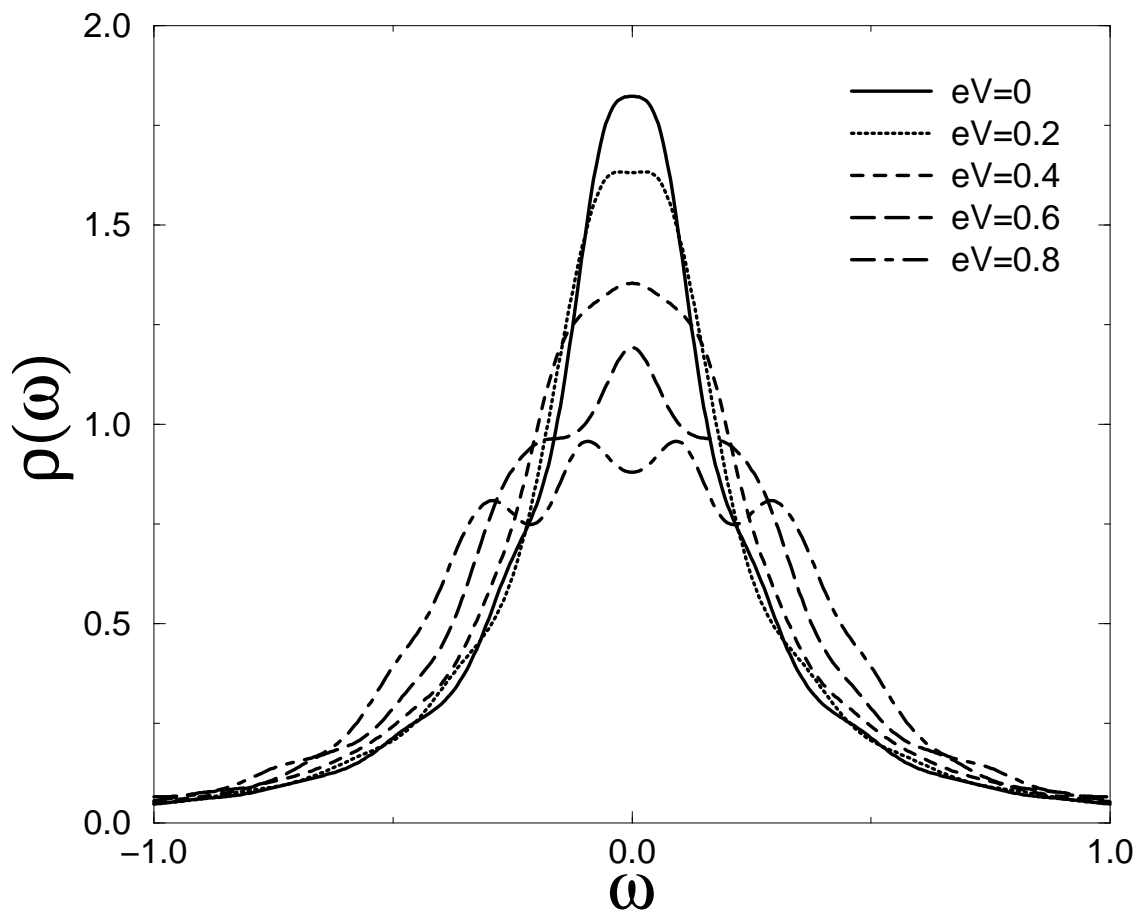


Figure 4: Local density of states at the impurity site (31) for $V_h = 0.3$ and $U = -0.2$.

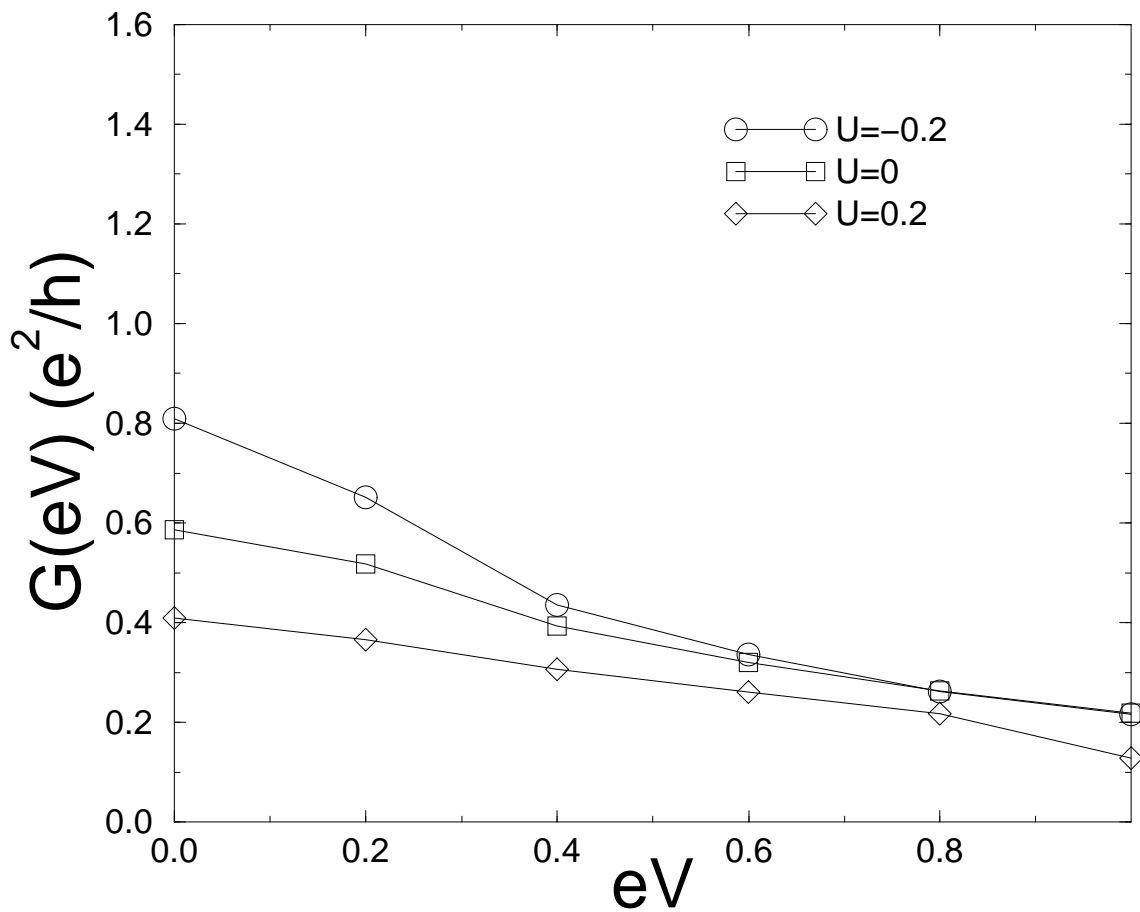


Figure 5: Differential conductance evaluated by means of the approximate formula (28) with our spectral-function data shown in Fig. 2-4. This is to be compared with the first-principle result shown in Fig. 1.